

Optical Vortex Filaments

Grover A. Swartzlander, Jr.
Physics Department
Worcester Polytechnic Institute
Worcester, MA 01609

This chapter examines the vortex core size and how it affects the propagation dynamics of neighboring optical vortices in the same beam. When the core is small compared to the distance between neighboring vortices, the vortices may be called vortex filaments. Such vortices have been found to exhibit unusual propagation dynamics such as rapid fluid-like vortex-vortex “effective interactions” [1,2]. In linear media this effect occurs over short propagation distances (compared to the diffraction length of the beam), whereas in nonlinear refractive (self-defocusing) media, the phenomenon may be sustained over longer distances [3] owing to the formation of optical vortex solitons [4]. Filament motion in the transverse plane depends on the distance from nearby vortices. In contrast large-core optical vortices move independently and relatively slowly (i.e., over length scales on the order of the diffraction length of the beam) [5]. Both large-core vortices and optical vortex solitons propagate as self-similar waves; hence, this greatly simplifies the mathematical analysis. However, vortex filaments in a linear material radiate diffraction rings and are significantly more difficult to treat. Here we present both ray-optics and physical optics descriptions for the latter case, i.e., for small-core vortices (within the paraxial approximation).

The Initial Field

From both experimental and theoretical points of view, the propagation dynamics of any beam depends on the initial conditions of the system. Here we describe the initial field of a system of entangled vortices in a single laser beam (this is different than a superposition of different beams containing vortices). Though the phase structure of an optical vortex spans the entire cross-sectional area of a beam (and beyond), we often describe the vortex as being located at a point called the *defect* where the intensity vanishes and the phase is undefined. Indeed, this point is the center of the vortex, located at the position \vec{R} in the x-y plane, as shown in Fig. 1. (For convenience, we adopt a notation where all displacement vectors are assumed to lie in the transverse (x,y) plane of the beam, and where the optical axis is co-linear with the z-axis.) In the vicinity of the defect the beam is characterized by a dark region of radius, w_v , called the *core*. By definition, the vortex imposes a phase over the entire beam which varies from

zero to an integer multiple of $\pm 2\pi$ around any closed path containing the defect. From a mathematical point of view, a vortex is essentially a separable complex factor, f , having an amplitude, A , an azimuthally harmonic phase, M , that spatially modifies the field of a carrier or “background” beam, G_{bg} , at each field point, \vec{r} :

$$f_j(\vec{r}, \vec{R}_j) = A_j \left(\left| \vec{r} - \vec{R}_j \right| \right) \exp(-iM_j \phi_j) \quad (1)$$

where the origin may be been assigned to the center of the beam (see Fig. 1), and each vortex in the beam is labeled with the subscript, j . In this chapter, we adopt a sign convention having a minus sign before M_j in Eq. (1) so that the azimuthal component of the wavevector, \vec{k} , is directed in the positive sense (counter-clockwise), as described

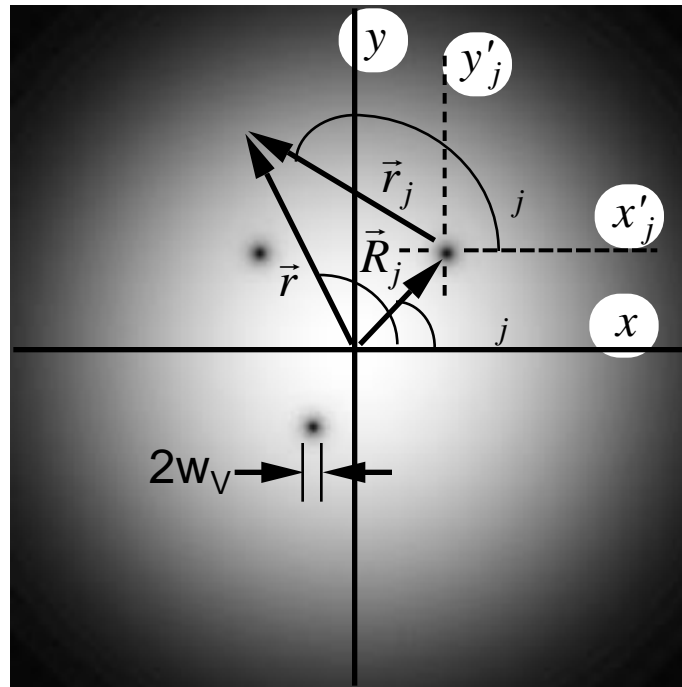


Figure 1. Intensity profile of a Gaussian laser beam containing multiple vortices located at the points (R_j, ϕ_j) $j = (1-3)$. At the field point (r, ϕ) , a distance, r_j , from the vortex core, the azimuthal angle circumscribing the vortex is ϕ_j .

below (see Eq. (24)). A given vortex has an integer topological charge or harmonic index, M_j , and an azimuthal angle defined around the defect: $\phi_j = \arctan(y_j/x_j)$, where $y_j = r \sin \phi_j - R_j \sin \phi_j$ and $x_j = r \cos \phi_j - R_j \cos \phi_j$ are the coordinates of the vector $\vec{r}_j = \vec{r} - \vec{R}_j$ pointing from the defect to an arbitrary point in the plane.

The fundamental units of topological charge are $M = \pm 1$, where $\sigma_j = \pm 1$. In general, any vortex having $|M| \geq 1$ may be represented as the product of “fundamental vortices”:

$$f_j(\vec{r}_j) = \prod_{l=1}^M A_l(r_j) \exp(-i l \phi_j) \quad (2)$$

where $\sigma_j = \pm 1$ is the sign of the j^{th} vortex and $r_j = |\vec{r}_j| = |\vec{r} - \vec{R}_j|$. Thus, the propagation dynamics of optical vortices may be described in terms of fundamental vortices.

If a thin transmissive mask is used to impose N vortices on a background beam having a transverse field profile, G_{bg} , the optical field immediately behind the mask may be written:

$$u(\vec{r}) = G_{bg}(\vec{r}) \exp[ikz - i \omega t] \prod_{j=1}^N f_j(r_j, \phi_j) \quad (3)$$

where ω is the angular frequency and $k = 2\pi/\lambda$ is the wavenumber, and λ is the wavelength of light. For convenience, we will drop the factor of $\exp[ikz - i \omega t]$ from expressions of the field. From Eq. (3) we see that the vortex factor, f , may be viewed as a filtering function that modifies the background beam. Note that Eq. (3) is not a linear superposition of separate vortex beams; rather it is an entanglement. Typical background beams used in experiments have a Gaussian profile centered at the origin ($\vec{r} = 0$). Assuming the background field has a flat initial phase profile, we write:

$$G_{bg}(\vec{r}) = E_0 \exp(-r^2/w_0^2) \quad (4)$$

where E_0 is the peak amplitude, w_0 , is the radial beam size (or “waist”), and $r = |\vec{r}|$.

In principle the initial amplitude profile of the vortex core, $A(r)$, may take any analytical form as long as Eq. (3) satisfies the wave equation. For example, waveguides and rough surfaces produce fields having the “natural” form $A_j = (r_j/L)^{|M_j|}$, where L is an arbitrary length parameter for coherent beams. In this chapter we are concerned with fundamental vortex filaments in the initial plane, and as a model equation, we choose

$$A_j(r_j) = \tanh(r_j/w_v) \quad (5)$$

where w_v is the characteristic vortex core size, as shown in Fig. 1. We note that when $w_v/w_0 \gg 1$, the core function converges to the natural form, $A_j = r_j/w_v$. In contrast, for $w_v \rightarrow 0$, we have a “point vortex”: $A_j(r_j) = 1$ for all $r_j > 0$, and $A_j(r_j = 0) = 0$. A point vortex initially has only phase structure, and therefore lends considerable analytical simplicity to a description of the initial propagation dynamics. In principle however, a point vortex is unphysical; though within the limits of the paraxial approximation ($w_v/w_0 \gg 1$), such structures may actually exist.

For example, computer-generated holograms may be used to create vortices [6,7] having arbitrary core functions [8] on a background beam. This requires one to numerically calculate the superposition of an “object wave” containing vortices with a “reference wave” (e.g., a tilted plane wave). The intensity profile (or interferogram) may be rendered as an image file, and transferred to an optically transmissive material such as acetate film. The interferogram of a distribution of N point vortices having arbitrary positions, core functions, and topological charges, is given by the modulus-squared field:

$$I(x,y) = \left| \exp(i2\pi x/\Lambda) + \sum_{j=1}^N A_j(r_j) \exp(-i\phi_j) \right|^2 \quad (6)$$

where the desired grating period, Λ , is usually selected to be several times the value of the resolution of the displaying or recording system. For example, the minimal dot size of a high-resolution laser printer is currently on the order of $5\mu\text{m}$.

The Optical Vortex Soliton

Driving the desire to create arbitrary distributions of optical vortices is the ability to experimentally observe optical vortex solitons [4] in self-defocusing media. The dynamics of vortex distributions is interesting in many fields of physical science, and computer-generated holography provides optics with unique experimental techniques not available in other fields. For example, optical vortex solitons are homologous with vortices in a superfluid, since both may be described to first order by the nonlinear Schrödinger equation; however, in optics the nonlinear control parameter (intensity) and the initial conditions may be directly and easily varied.

The core function of an OVS does not have a closed form solution, but may be

$$w_v = 1.27k^{-1}(n_0/n_{NL})^{1/2}$$

represented by Eq. (5) near the core, where $w_v = 1.27k^{-1}(n_0 / n_{NL})^{1/2}$ and $n_{NL} = -n_2|E|^2$ is the intensity-dependent change of the refractive index for a material having a negative nonlinear coefficient, $n_2 < 0$. The primary difference between OVS's and vortices in linear media is that the core does not diffract in the nonlinear case; that is, linear diffraction is counterbalanced by nonlinear refraction. Vortex propagation dynamics is affected by the overlapping cores of other vortices [1], and thus, the ability to maintain a constant core size may allow enhanced effective interactions between vortices.

We have proposed possible applications of OVS's, including dynamic waveguiding, optical modulators and transistors, and image enhancement schemes. The OVS induces a cylindrical graded-index waveguide in the nonlinear material, $n(r)/n_0 = 1 - (n_2/n_0)|E_0|^2 \tanh^2(r/w_v)$, and a second laser beam may be guided by the vortex beam [4,9]. This index profile may be viewed as an optical fiber with cladding, $n_{clad} = n_0 + n_2|E_0|^2$, and a core $n_{core} = n_{clad} - n_2|E_0|^2 \operatorname{sech}^2(r/w_v)$.

Additional all-optical or electro-optical techniques may be used to modulated the waveguide, and thus modulate the guided beam or amplify an optically encoded signal [10]. Nonlinear filtering techniques based on the intensity-dependent vortex core size may be used to resolve two closely spaced defects in a phase image. Furthermore, linear filtering using a vortex phase mask may be used to detect edges in an image.

The Propagating Field

Upon passing a laser beam through a vortex mask or hologram, one obtains a field described by Eq. (3). The propagation dynamics of the system of vortices may be easily recorded by translating a CCD camera along the optical axis. For point vortices, one finds that the cores immediately begin to move in the plane while also radiating high spatial frequency diffraction rings [1,3,8]. This radiation phenomenon may be readily understood by calculating the propagating field of a point vortex of charge m located at the center of a planar Gaussian beam. In general, the propagating field may be expressed in cylindrical coordinates [11] whereby the Fresnel integral may be written as a Hankel transform, H_m [12]:

$$u(r, z) = (2 / i z) \exp[-im(\theta + \phi/2)] \exp[ikr^2 / 2z] H_m \{ h(r) \exp(-r^2 / w_0^2) \} \quad (7)$$

where $h(r) = \exp[i(k/2z)r^2]$ is the field propagator,

$$H_m\{g(r)\} = \int_0^{\infty} r g(r) J_m(rrk/z) dr \quad (8)$$

and J_m is the Bessel function:

$$J_m(a) = (2/a)^{-1} \int_0^a d \exp[-im(\theta + \pi/2)] \exp[-ia \cos \theta] \quad (9)$$

Propagation of a Point Vortex

Evaluating Eq. (7) for a point vortex on a Gaussian background field, we find the vortex charge is a constant of motion (as expected from the principle of conservation of orbital angular momentum), and the solution may be written in the separable form [3,8]:

$$u(r, z) = A_m(r, z) \exp[-im\theta] \exp[i\phi_m(r, z)] \quad (10)$$

where

$$A_m(r, z) = \frac{\sqrt{r}}{2} \frac{r}{w_0} \frac{z_0}{z} \frac{z_0}{R(z)} \exp\left[-\frac{1}{2} \frac{r^2}{w(z)^2}\right] \left[I_{\frac{m-1}{2}}\left(\frac{r}{z}\right) - I_{\frac{m+1}{2}}\left(\frac{r}{z}\right) \right] \quad (11a)$$

and

$$\phi_m(r, z) = -m\frac{\theta}{2} + \frac{\pi}{4} + \frac{r}{w_0} \frac{z_0}{z} \left[1 - \frac{w_0^2}{2w(z)^2} \right] - \frac{3}{2} \tan^{-1} \frac{z}{z_0} \quad (11b)$$

where $\theta = (1/2)(r/w(z))^2(1+iz_0/z)$, $w(z) = w_0[1+(z/z_0)^2]^{1/2}$, and $R(z) = z(1+(z_0/z)^2)$. The intensity profile, A_m^2 , is shown in Fig. 2 for various propagation distances. We see that within one diffraction length, $z_0 = (1/2)kw_0^2$, the diffraction rings have radiated away from the intense regions of the beam, and the vortex core has broadened to $w_v = 0.54w_0$. In the far-field region, the core subtends a finite angle and the diffraction rings disappears.

Except for the step amplitude singularity in the initial plane, we have shown that a diffracting point vortex is a well-behaved function within the context of the paraxial approximation. Both the near-field and far-field profiles may be expressed in terms of tabulated integral functions for arbitrary integer values of m .

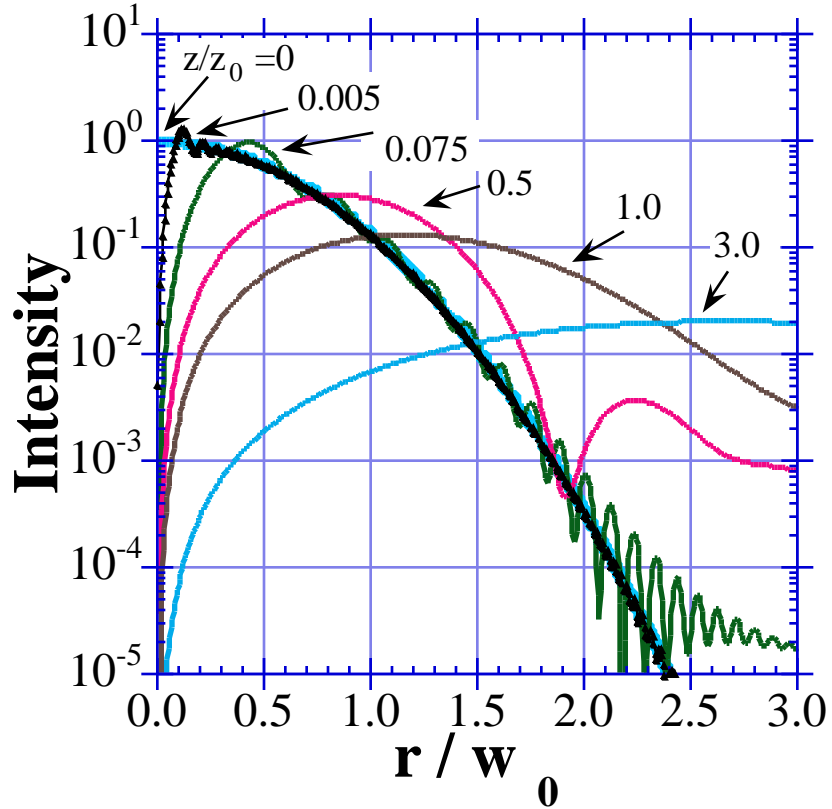


Figure 2. Radial intensity distributions (log intensity scale) of a Gaussian background beam initially containing a point vortex in the plane, $z/z_0 = 0$. High spatial frequency radiation from the vortex core becomes negligible for $z/z_0 > 1$.

Far-Field Distribution of a Point Vortex

An understanding of the far-field beam profile of a vortex is particularly important in applications such as optical trapping [13-15], optically induced rotation [16], and spatial filtering [8]. In these applications the far-field profile occurs in the vicinity of the focal plane of a lens. In a Fourier transforming optical system with the vortex mask in the front focal plane of a lens of focal length f , the far-field pattern appears in the back focal plane [11]. The fields in these two planes are related by Fourier and inverse Fourier

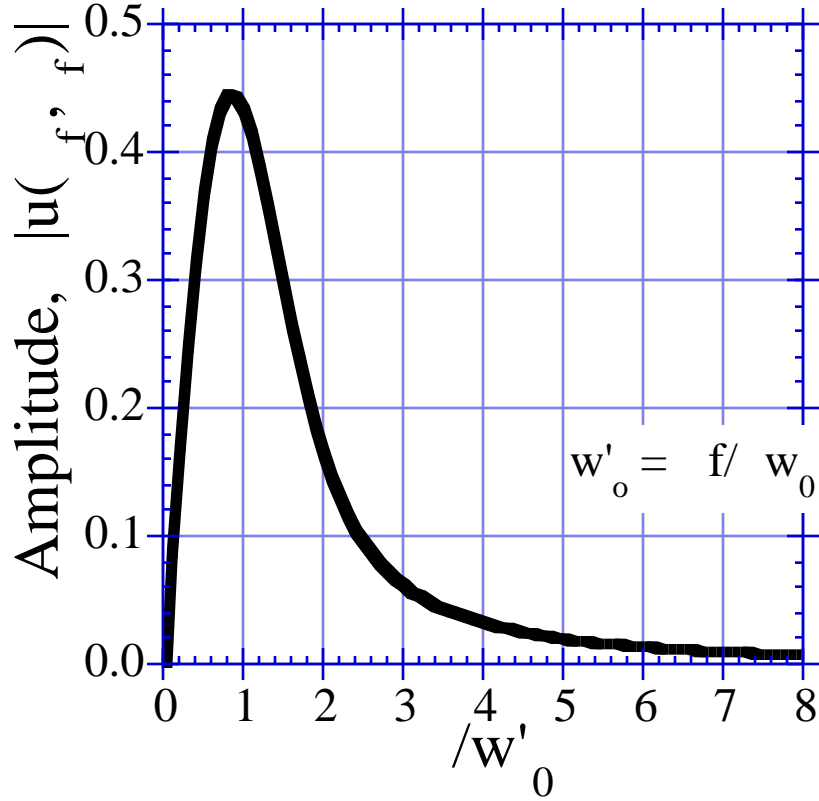


Figure 3. Amplitude profile in the Fourier transform plane of a lens. The initial beam in the conjugate plane contains a point vortex on a Gaussian background beam. w_0 is the diffraction-limited focal spot size.

transforms. For a single point vortex on a Gaussian background field, the optical field in the back focal plane, $u_f(r_f, f)$, may be determined from the equation:

$$u_f(r_f, f) = (-ik/f) \exp[-im(r_f - \lambda/2)] \int_0^\infty \exp[-r^2/w_0^2] J_m(kr_f/f) r dr \quad (12)$$

where the two-dimensional Fourier integral has been written as a Hankel transform. Evaluating the integral, one obtains:

$$|u_f(r_f, f)| = \frac{1}{2} \frac{z_0}{f} \frac{f}{w_0} \exp[-\dots] \left[I_{m-1}(\dots) - I_{m+1}(\dots) \right] \quad (13)$$

where $\dots = (1/2)(r_f/w_0)^2$ and $w_0 = f/w_0$ is the characteristic size of the focused beam. The field profile, shown in Fig. 3, is a smooth function (as expected from the discussion of Fig. 2) having a core size of $w_v \approx 0.4w_0$ (this is roughly the half-width at

half-maximum of the peak intensity). Furthermore, we find that the tail of the amplitude profile decreases as r^{-2} for large values of r/w_0 .

Delta Function Representation

As another important example, let us examine the far-field distribution for a fundamental vortex ($m=1$) on a planar background field. In this case we evaluate Eq. (12) in the limit, $r/w_0 \gg 1$, where $I_{0,1}(r) \approx (2/r)^{1/2} [\exp(r) \pm i \exp(-r)] \times (1 + O(1/r))$ [17], and we find

$$\lim_{r/w_0 \gg 1} u_f(r, r) \Big|_{m=1} \approx -(w_0^2/r) \exp(-i r) \exp[-(r/w_0)^2] \quad (14a)$$

In this limit, the transformed waist tends to vanish: $w_0 = r/w_0 \rightarrow 0_+$. However, at the origin where $r/w_0 = 0$, the vortex field must also vanish. Thus, for a point vortex on an otherwise planar background field of infinite extent, one may approximate the far-field distribution as a delta function:

$$u_f(r, r) \Big|_{m=1} \sim \exp[-i r] \frac{d}{dr} \delta(r) \quad (14b)$$

where $\delta(r)$ is the Dirac delta function of the far-field radial coordinate, r . In fact, numerical analysis qualitatively shows that Eq. (14b) is a better approximation of Eq. (12) than Eq. (14a) in this limit. We shall see that this symbolic delta function representation is important in understanding the qualitative affect that vortices have on the far-field distributions of background beams. For example, according to the convolution theorem of Fourier transforms, Eq. (12) may be approximated by the convolution of Eq. (14b) with a Gaussian distribution, resulting in the derivative of a Gaussian distribution. An inspection of Fig. 3 confirms this estimate, except in the region of the slowly decaying tail.

An Arbitrary On-Axis Vortex

Let us now consider an arbitrary vortex having a non-zero core size. Formally one may evaluate the expression for the propagating field:

$$u(r, \theta, z) = (2 / i z) \exp[-im(\theta + \phi/2)] \exp[ikr^2 / 2z] H_m \{ h(r) A(r) \exp(-r^2 / w_0^2) \} \quad (15)$$

Using principles of Fourier optics [11,12], however, the field may also be determined from a convolution integral. From this point of view, one may expect the optical field in the focal plane of a lens,

$$u_f(r_f, \theta_f) = (-ik / f) \exp[-im(\theta_f - \phi/2)] \int_0^\infty A(r) \exp[-r^2 / w_0^2] J_m(kr_f / f) r dr \quad (16)$$

to be similar to Eq. (13), except the distribution (Eq. (16)) will be broadened owing to the convolution with the Fourier transform of the core function, $FT\{A(r)\}$.

Thus, a qualitative understanding of the far-field distribution may be obtained by first determining the field for a point vortex on an infinite background, and then convolving this result with the Fourier transform of the actual background and core:

$$u_f(r_f, \theta_f) \sim \exp(-im\theta_f) \times \int_0^\infty J_m(kr_f / f) r dr \quad FT[A(r) \exp(-r^2 / w_0^2)] \quad (17)$$

Similar to the arguments leading to Eq. (14b), the integral in Eq. (17) may be approximated (for the case $m=1$) by the convolution of $d(r_f) / d_f$ with $FT[A(r) \exp(-r^2 / w_0^2)]$. This suggests that the integral is roughly equal to the derivative of the distribution, $FT[A(r) \exp(-r^2 / w_0^2)]$, with respect to the far-field coordinate, r_f . This operation is depicted in Fig. 4.

An Off-Axis Vortex

Let us consider an arbitrary background beam, $g(r, \theta)$, centered on the optical axis, having a singly charged off-axis vortex, $\exp(-i\theta)$, at the point (R, θ) , where $\theta = \pm 1$. The coordinates (r, θ) and (R, θ) , shown in Fig. 1, are related by the relation

$$r \exp(-i\theta) = r \exp(-i\theta) + R \exp(-i\theta) \quad (18)$$

The far-field beam profile, u_f , may be computed by taking the Fourier transform of the initial beam:

$$u_f = FT\{g(r, \theta) A(r) \exp(-i\theta)\} = FT\{g(r, \theta) A(r) r^{-1} [r \exp(-i\theta) - R \exp(-i\theta)]\} \quad (19)$$

where $FT\{\}$ represents the Fourier transform operation.

Considerable simplification is obtained for a natural core function, $A(r) = r/L$:

$$u_f = \text{FT}\{g(r, \theta)(r/L)\exp(-i\theta)\} - (R/L)\exp(-i\theta) \text{FT}\{g(r, \theta)\} \quad (20)$$

where L is an arbitrary length. The final term in Eq. (20) may be viewed as a “sifting” property of the Fourier transform of a displaced vortex. A Gaussian background beam (Eq. (4)) allows additional simplification because tabulated integrals [18] may be used to evaluate Eq. (20) and thereby determine the far-field position of the vortex.

For example, in the back focal plane of a Fourier transforming optical system, as discussed above, the field may be computed for any value of $m > -1$:

$$\begin{aligned} & \text{FT}\{G_{bg}(r)(r/L)^{|m|} \exp(-im\theta)\} \\ &= (-ik/Lf)\exp(-im(\theta_f^{(1)} - \theta/2)) \int_0^\infty G_{bg}(r)(r/L)^{|m|} J_m(k_f r/f) r dr \quad (21) \\ &= (-ik/f)\exp(-im(\theta_f^{(1)} - \theta/2)) \frac{r_f w_0}{L w_0} \frac{w_0^2}{2} \exp(-r_f^2/w_0^2) \end{aligned}$$

where $w_0 = f/w_0$ is the waist of the focused beam. For $m = -1$ we must use the identity $J_{-m} = (-1)^m J_m$.

The location $(R_f^{(1)}, \theta_f^{(1)})$ of the single displaced vortex in the Fourier transform plane may be determined by substituting Eq. (21) into Eq. (20) for the cases $m = 1$ and $m = 0$, and then setting Eq. (20) to zero. We find that

$$(R_f^{(1)}, \theta_f^{(1)}) = (R w_0 / w_0, \theta + \theta/2) \quad (22)$$

and thus, the far-field vortex maintains its relative radial position from the center of the beam (i.e., $R_f^{(1)} / w_0 = R / w_0$), whereas the angular position is shifted by $\theta/2$.

Using numerical techniques, one may readily verify [3] that the far-field position, $(R_f^{(1)}, \theta_f^{(1)})$ of a single vortex of arbitrary charge, m , and arbitrary vortex core function, $A(r)$, on a Gaussian background beam is given by Eq. (22), provided the function depends only on the radial position from the core and is everywhere positive. For example, Fig. 4 shows the near and far field intensity profiles of off-axis vortices having natural and point-like core functions. In both cases the coordinates of the far-field vortices are given by Eq. (22). The convolution relation, described by Eq. (17), is also depicted in the figure.

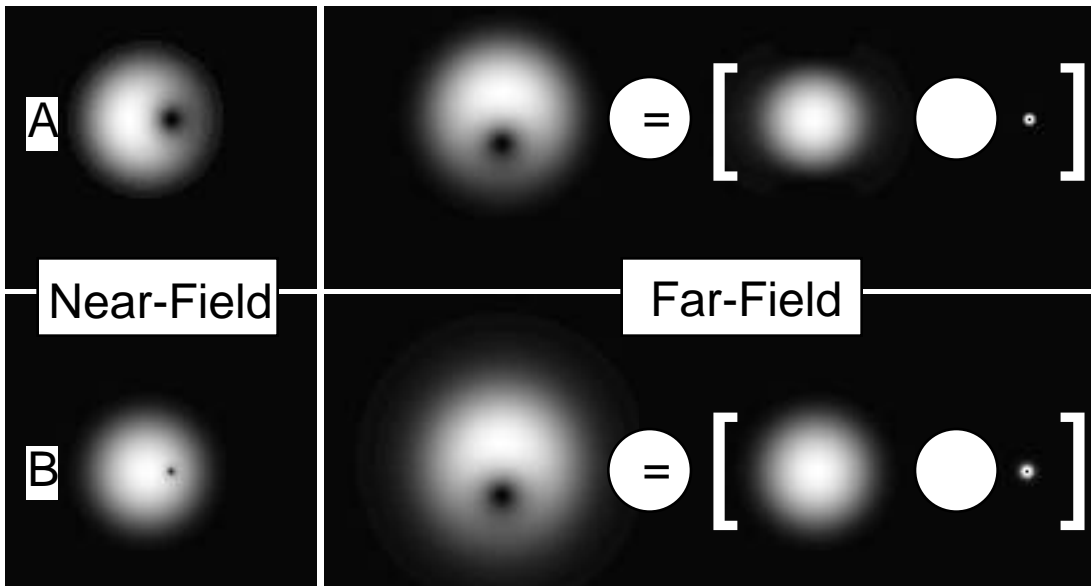


Figure 4. Near and far-field intensity profiles for a single large and small core vortex ($m = 1$) on a Gaussian beam. The position of the far-field vortex is independent of the core size when a single vortex is present. The far-field distribution is depicted as the convolution of the amplitude of the combined core and background function with a two-dimensional delta function.

Two Off-Axis Vortices

Having developed an understanding of the near and far-field properties of a single vortex, let us now examine the propagation dynamics of two or more vortices in a single beam, as may be described using Eq. (3). In particular, let us focus our attention on vortex filaments, whose size, w_v , is much smaller than the beam size, w_0 , and also much less than the distance between nearest-neighbor vortices, d , (e.g., $w_v \ll d$). It has been shown that an effective interaction exists between such vortices, analogous to the motion of vortex filaments in a fluid [1-3]. That is, as the vortices propagate through space, their transverse motion is determined in part by the “flow” established by other vortices in the beam. In optics, this flow is established by the direction of the wavefronts. That is, light tends to move in the direction normal to the local wavefront. For example, if the transverse phase of the beam is given by Eq. (2), then the initial net phase across a beam containing N vortices may be written:

$$\vec{k}_{net} = \sum_{j=1}^N \vec{k}_j \quad (23)$$

As the beam propagates, the phase will develop complicated structure; however, such higher-order effects may be ignored for propagation distances less than the characteristic diffraction length corresponding to the vortex separation distance, namely, $z_V = (1/2)kd^2$.

The ray-optics model may be used when the diffraction effects are ignored, and the ray trajectories are simply given by the gradient of the phase. Assuming paraxial rays, we are only concerned with the transverse wavevectors, which may be expressed:

$$\vec{k}_{net} = - \sum_{j=1}^N \frac{\hat{e}_j}{r_j} \quad (24)$$

where \hat{e}_j is the azimuthal unit vector circumscribing the j^{th} vortex. At the center of the j^{th} vortex ($r_j = 0$), \hat{e}_j is undefined, and the momentum of a ray at that point is independent of the vortex charge, q_j . For a single vortex, $N = 1$, Eq. (24) predicts that a pencil of rays will initially tend to circumnavigate the vortex core, while the core itself is stationary. For $N = 2$, the core of one vortex is displaced along an arc of radius d measured from the other vortex. When $q_1 = q_2$, the two vortices tend to orbit the midpoint between them, whereas when $q_1 = -q_2$, the vortices tend to move along parallel trajectories that are perpendicular to a line connecting the two vortex cores. This is analogous to the dynamics of vortex filaments in a fluid [19]. Until recently, however, this effect was not observed in optics because optical vortex filaments were not investigated; rather, only large-core vortices were examined. Therefore, let us closely examine the propagation of two vortex filaments.

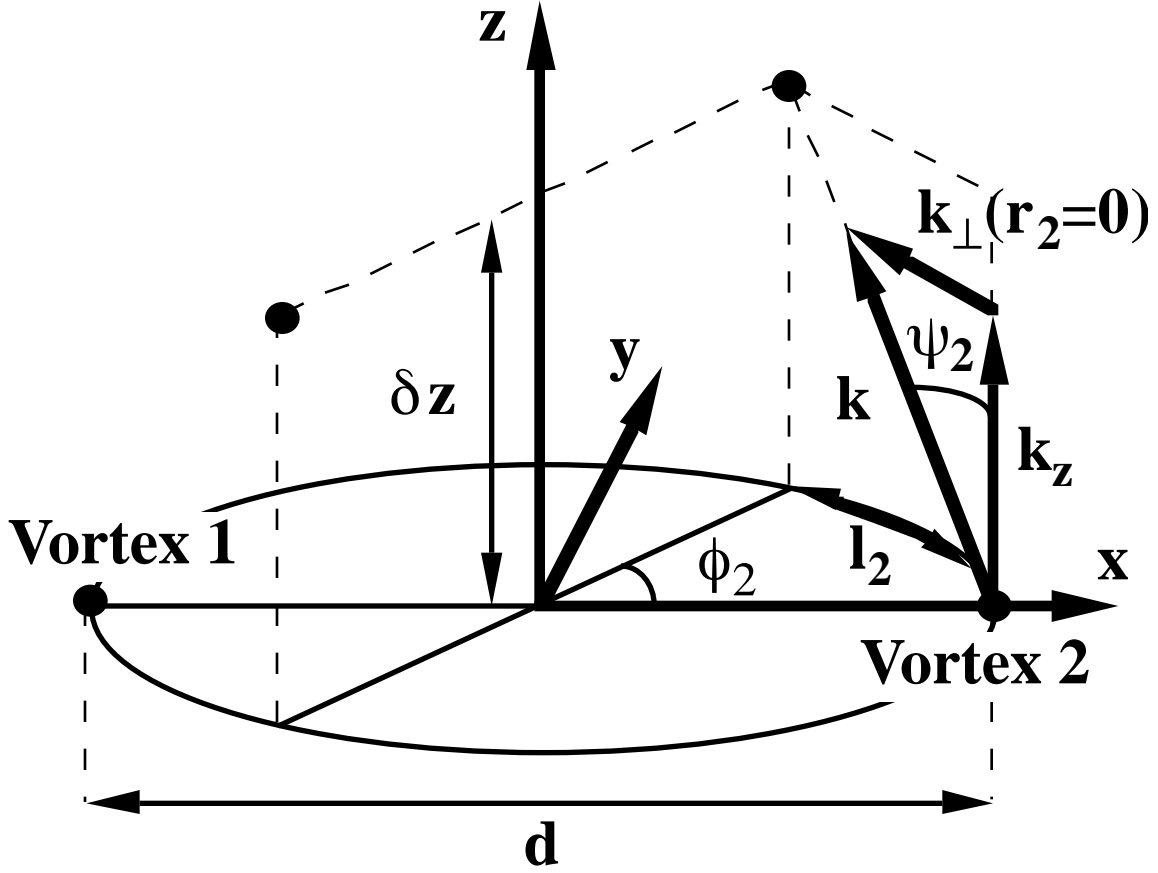


Figure 5. Position and wavevectors of two vortices separated by a distance, d in the x - y plane. The only phase and wavevector at the defect point of vortex-2 is that of vortex-1. After propagating a small distance, z , the vortices rotate to new positions which, when projected on the transverse plane are displaced by the arclength, l

In the near-field region, $|z| < z_v$, the transverse momentum at the center of vortex-1 and vortex-2 is given, respectively, by

$$\vec{k}(r_1=0) = -\hat{e}_2 / r_2, \quad \vec{k}(r_2=0) = -\hat{e}_1 / r_1 \quad (25)$$

where $r_1 = r_2 = d$. The rays have azimuthal components of momentum because the wavefront of each vortex is helical (i.e., the three-dimensional surface of constant phase, $-m\phi + kz = \text{const}$, is a helix). The ray at the center of vortex-2 will project an arc in the transverse plane as it propagates, as shown in Fig. 5. The arclength is given by $l_2 = z \tan \psi_2 = (d/2) \tan \psi_2$, where the angle ψ_2 subtends the transverse and longitudinal wavevectors:

$$\tan \psi_2 = k(r_2=0) / k_z = l_2 / d \quad (26)$$

where we assume the paraxial approximation, $k \ll k_z \approx k$. The initial angular rate of rotation of vortex-2 about the optical axis is therefore given by

$$|\dot{\phi}_v| = d\phi_2/dz = \dot{\phi} / d^2 = 1/z_v \quad (27)$$

Repeating the calculations for vortex-1 we obtain the same initial rate. Thus, when $\phi_1 = \phi_2$ both vortices rotate about a common axis in the (counter-)clockwise sense when $(\phi_1 = -1) \phi_2 = 1$. In contrast, when $\phi_1 = -\phi_2$ the vortices both follow a linear trajectory in the $\pm \hat{y}$ direction if $\phi_1 = \pm 1$. Thus, the kinematics of a pair of optical vortex filaments is analogous to that of vortex filaments in a fluid. In optics, however, the filaments diffract as they propagate, and experimental [1] and numerical [3] investigations confirm that the fluid analogy fails over propagation distances exceeding $\sim z_v/4$. Thus far we have ignored the effects of an amplitude gradient on the vortex motion. As the radiation from one vortex diffracts past the other core, the vortices experience a radial “force”. For example, when the vortices have the same topological charge, this diffraction pushes them away from each other, which tends to retard the angular rate of rotation. Furthermore, once the cores overlap, the effective interaction between the vortices vanishes.

Numerically calculated near and far-field intensity profiles for point vortices on a Gaussian background beam are shown in Fig. 6 for eight different cases: (A) one defect in center of beam, (B) one off-axis defect, (C) two closely spaced vortices of opposite charge, (D) two identical closely spaced vortices, (E) two moderately spaced vortices of opposite charge, (F) two identical moderately spaced vortices, (G) two largely spaced vortices of opposite charge, (H) two identical largely spaced vortices. In all cases the far-field profiles (A2, B2, ..., H2) are characteristically large cores than the near field profiles.

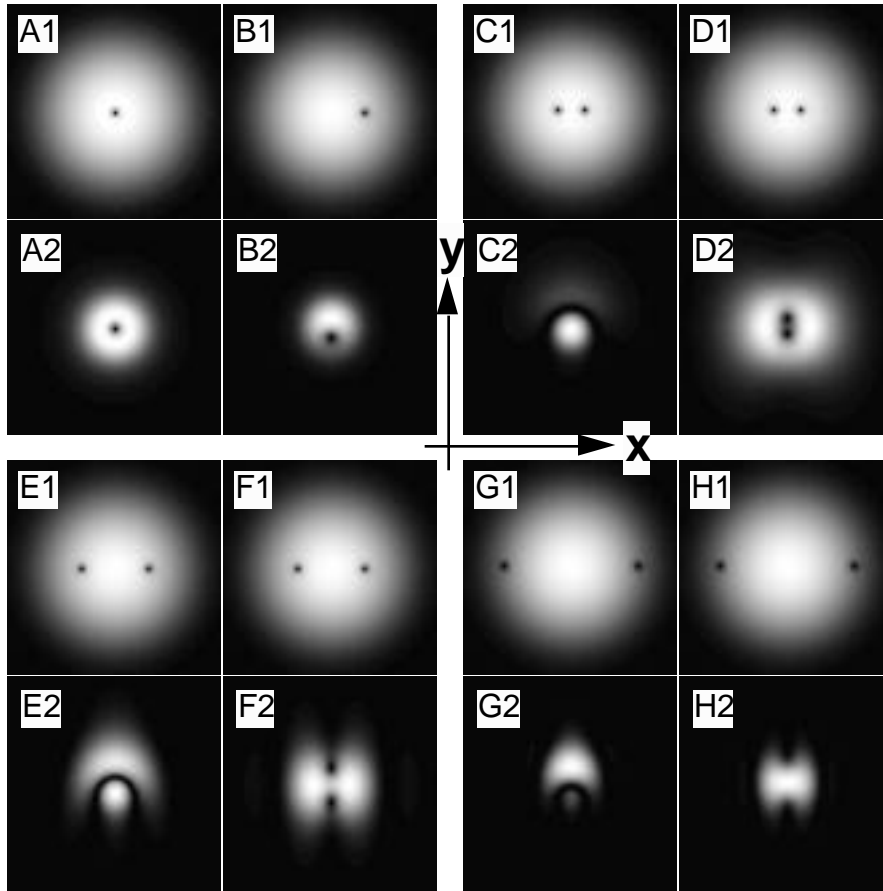


Figure 6. Near (1) and far (2) field intensity profiles for single vortices (A,B), vortices of opposite charge (C,E,G), and vortices of equal charge (D,F,H).

Arbitrary Number of Vortices and Arbitrary Core Functions

The far-field profile for any number of vortices having arbitrary core functions, topological charge, and background fields, may be written:

$$\begin{aligned}
 u_f &= \text{FT} \left\{ g(r) \prod_{j=1}^N A_j(r_j) \exp(-i \phi_j) \right\} \\
 &= \text{FT} \left\{ g(r) \prod_{j=1}^N \frac{A_j(r_j)}{r_j} \prod_{l=1}^N r_l \exp(-i \phi_l) \right\} \quad (28) \\
 &= \text{FT} \left\{ g(r) \left(\prod_{j=1}^N A_j(r_j) \right) \left(\prod_{l=1}^N r_l \right) \right\}
 \end{aligned}$$

where $\prod_{j=1}^N (r_j)^{-1} A_j(r_j)$ and $\prod_{l=1}^N r_l \exp(-i \phi_l)$. Using the convolution relation of the Fourier transform of a product of functions, Eq. (28) may be written

$$u_f = \tilde{g} - \tilde{w} \quad (29)$$

where $\tilde{g} = \text{FT}\{g\}$, $\tilde{w} = \text{FT}\{w\}$, $\tilde{w}_0 = \text{FT}\{w_0\}$.

As an example, consider the case $N = 1$. One may readily determine the position of the defect by using Eq. (18) and then setting Eq. (29) to zero.

$$u_f = \tilde{g} - \tilde{w} \left[\text{FT}\{r \exp(-i k_f r)\} - R \exp(-i k_f r) \right] \quad (30)$$

Assuming that the background field, g , and the modified core function, $(r)^{-1}A(r)$, are everywhere real positive definite functions (and obviously even functions), then we note that $\tilde{g} - \tilde{w}$ is also everywhere a real positive definite (even) function. The first term in the square bracket is undefined, but may be understood in terms of Eq. (14a) in the limit as $w_0 \rightarrow 0$, i.e., Eq. (14b). Thus the bracketed factor in Eq. (30) may be represented as $\sim \exp(-i k_f r) d \left(\frac{A(r)}{r} \right) / d_f - \text{const}$, and acts as a comparator of the derivative of $\tilde{g} - \tilde{w}$ and the complex constant times $\tilde{g} - \tilde{w}$. At the point where the two are equal, Eq. (30) vanishes, and the far-field defect appears. For $N > 1$ the function \tilde{w} contains cross-terms which complicate the description of the positions of the defect. Our numerical studies indicate that the position of the far field defects do not coincide when $N > 1$.

Acknowledgments

This work was supported by a grant from the Research Corporation (Cottrell Scholars Award) and the National Science Foundation (Young Investigator Award). I acknowledge insightful discussion with C. T. Law (University of Wisconsin at Milwaukee), and my present and former students D. Rozas and Z. S. Sacks.

References

- [1]. D. Rozas, Z.S. Sacks, and G.A. Swartzlander, Jr., "Experimental observation of fluid-like motion of optical vortices," *Phys. Rev. Lett.* **18**, 3399-3402 (1997).
- [2]. F.S. Roux, "Dynamical behavior of optical vortices," *J. Opt. Soc. Am. B* **12**, 1215-1221 (1995).
- [3]. D. Rozas, C.T. Law, and G.A. Swartzlander, Jr., "Propagation dynamics of optical vortices," *J. Opt. Soc. Am. B* **14**, 3054-3065 (1997).
- [4]. G.A. Swartzlander, Jr. and C.T. Law, "Optical vortex solitons observed in Kerr nonlinear media," *Phys. Rev. Lett.* **69**, 2503-2506 (1992).
- [5]. G. Indebetouw, "Optical vortices and their propagation," *J. Opt. Soc. Am. B* **40**, 73-87 (1993).

- [6]. V.Yu. Bazhenov, M.V. Vasnetsov, and M.S. Soskin, "Laser beams with screw dislocations in their wavefronts," *Pis'ma Zh. Eksp. Teor Fiz.* 52, 1037-1039 (1990) [*JETP Lett.* 52, 429-431 (1990)].
- [7]. N.R. Heckenberg, R. McDuff, C.P. Smith, and A.G. White, "Generation of optical phase singularities by computer-generated holograms," *Opt. Lett.* 17, 221-223 (1992).
- [8]. Z.S. Sacks, D. Rozas, and G.A. Swartzlander, Jr., "Holographic formation of optical vortex filaments," *J. Opt. Soc. Am. B* 15, 2226-2234 (1998).
- [9]. A.W. Snyder, L. Poladian, and D. J. Mitchell, "Stable black self-guided beams of circular symmetry in a bulk Kerr medium," *Opt. Lett.* 17, 789-791 (1992).
- [10]. G.A. Swartzlander, Jr., D.L. Dragan, N. Hallak, M.O. Freeman, and C.T. Law, "Optical transistor effect using an optical vortex soliton," *Laser Physics* 5, No. 3, 704-709 (1995).
- [11]. J.W. Goodman, Introduction to Fourier Optics (McGraw-Hill, New York, 1968).
- [12]. J.D. Gaskill, Linear Systems, Fourier Transforms, and Optics (John Wiley & Sons, New York, 1978).
- [13]. A. Ashkin, "Forces of a single-beam gradient trap on a dielectric sphere in the ray optics regime," *Biophys. J.* 61, 569-582 (1992).
- [14]. H. He, N.R. Heckenberg, and H. Rubinsztein-Dunlop, "Optical particle trapping with higher-order doughnut beams produced using high efficiency computer generated holograms," *J. Mod. Opt.* 42, 217-223 (1995).
- [15]. K.T. Gahagan and G.A. Swartzlander, Jr., "Optical vortex trapping of particles," *Opt. Lett.* 21, 827-829 (1996).
- [16]. H. He, M.E.J. Friese, N.R. Heckenberg, and H. Rubinsztein-Dunlop, "Direct observation of transfer of angular momentum to absorptive particles from a laser beam with a phase singularity," *Phys. Rev. Lett.* 75, 826-828 (1995).
- [17]. I.S. Gradshteyn and I.M. Ryzhik, *Table of Integrals, Series, and Products*, (Academic Press, New York, 1980), p. 962, Eq. 8.451.5.
- [18]. *ibid*, p. 717, Eq. 6.631.4
- [19]. A. Sommerfeld, Mechanics of Deformable Bodies, (Academic Press, New York, 1950).